THE JOURNAL OF PHYSICAL CHEMISTRY B

Article

pubs.acs.org/JPCB

Ultraviolet-Tunable Laser Induced Phototransformations of Matrix Isolated Isoeugenol and Eugenol

J. Krupa,[†] A. Olbert-Majkut,[†] I. Reva,*[,‡] R. Fausto,[‡] and M. Wierzejewska*[,†]

[†]Faculty of Chemistry, University of Wrocław, Joliot-Curie 14, 50-383 Wrocław, Poland

[‡]Department of Chemistry, University of Coimbra, 3004-535 Coimbra, Portugal

Supporting Information

ABSTRACT: In situ photochemical transformations of monomers of 2-methoxy-4-(prop-1-enyl)phenol (isoeugenol) and 2-methoxy-4-(prop-2-enyl)phenol (eugenol) isolated in low temperature matrices were induced by tunable UV laser light, and the progress of the reactions was followed by FTIR spectroscopy. Conformer-selective $E \leftrightarrow Z$ geometrical isomerizations could be successfully induced by irradiation at different wavelengths from the 310−298 nm range in the isoeugenol molecule, contains an asymmetrically substituted exocyclic C=C bond. Photolysis of both studied compounds was also observed, with H-atom shift from the OH group and formation of two types of long-chain conjugated ketenes. The photoproduced ketenes were found to undergo subsequent photodecarbonylation. Interpretation of the observed photoprocesses was supported by quantum chemical calculations undertaken at different levels of theory (DFT, MP2, QCISD).

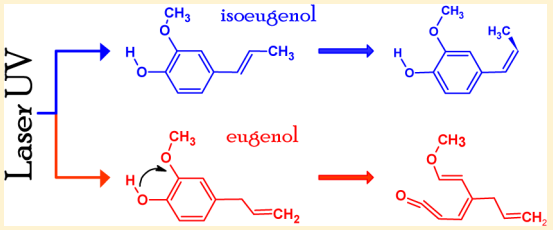

INTRODUCTION

Given their unique properties as antioxidants and free radical scavengers, plant phenols have garnered the attention of scientists interested in the elucidation of many aspects of their biological activity. More recently, plant phenols have also gained increasing interest as multipurpose functional agents.[1−8]

The most known plant phenols, including the propenylphenols (such as isoeugenol, anol) and the allylphenols (eugenol, chavicol) as well as their derivatives, are aromatic constituents of essential oils. Many studies have been reported that focused on plant phenols in essential oils from the viewpoint of their flavor and fragrance chemistries.[9,10] On the other hand, most of the studies reporting medical properties of plant phenols deal with multicomponent samples. They are subjected to inherent intraspecific variability of the composition—depending on location, meteorology, and many other factors, making the obtained results irreproducible.[11] From this point of view, small phenolic compounds such as eugenol and isoeugenol may serve as suitable molecular models in fundamental studies useful to understand the bioactivity of plant phenols in relation to their structural preferences. In addition, many phenolic compounds present in plants are known to play an important role as effective antioxidant and radical-scavenging agents as well as UV absorbers.

Although the conformational preferences and photochemical properties of the plant phenols can be expected to be fundamental in determining their biological activity, not much data on these subjects are available in the literature. The infrared spectrum of guaiacol (2-methoxyphenol), its self-association, and complexes with nitrogen were studied by the matrix isolation technique by Tylli and Konschi,[12] and the molecular structures and preferred conformations of a series of substituted methoxyphenols were investigated by Wu and Brutschy, using resonant two-photon ionization infrared spectroscopy (R2PI/IR),[13] and by Dorofeeva et al., using gas-phase electron diffraction and quantum chemical calculations.[14] In turn, the conformational landscape of eugenol (2-methoxy-4-(prop-2-enyl)phenol), one of the most important plant phenols, was investigated by matrix isolation infrared spectroscopy by Olbert-Majkut and Wierzejewska,[15] allowing for unequivocal identification and spectral characterization of three different eugenol conformers. Eugenol in a supersonic expansion was also studied by several complementary laser spectroscopic methods by Longarte et al.,[16] the two most stable conformers of the molecule being detected under the experimental conditions used. Finally, formation of *Z*-anethole (1-methoxy-4-[(*Z*)-prop-1-enyl]benzene) and various dimers, as a result of the exposure of *E*-anethole to UV−vis irradiation, was established by means of high resolution gas chromatography coupled to mass spectrometry in a recent study of Castro, Martínez, and Stashenko.[17]

In the present article, we describe our studies on the laser-induced phototransformations of two important plant phenols, isoeugenol (2-methoxy-4-(prop-1-enyl)phenol; IE) and eugenol (2-methoxy-4-(prop-2-enyl)phenol; EU), isolated in low temperature matrices. The studied molecules (IE and EU) are presented in Chart 1. As will be described in detail below, in case of the asymmetrically substituted around the exocyclic C=C bond isoeugenol molecule, conformer-selective $E \leftrightarrow Z$ geometrical isomerizations could be successfully promoted

Received: June 27, 2012
Revised: July 24, 2012
Published: July 24, 2012

   dx.doi.org/10.1021/jp306339g | *J. Phys. Chem. B* 2012, 116, 11148−11158

Chart 1. Schematic Representation of IE and EU

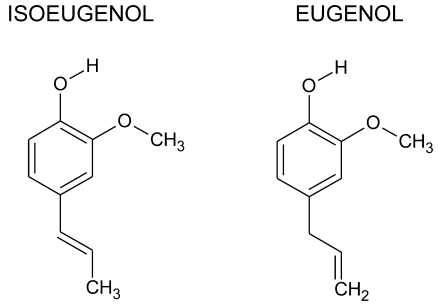

upon irradiation at different wavelengths in the 310−298 nm range. Photolysis of both studied compounds was also observed, with an H-atom shift from the OH group and formation of two types of long-chain conjugated ketenes.

EXPERIMENTAL AND THEORETICAL METHODS

Matrix isolation FTIR Studies and Irradiation Experiments. Isoeugenol (IE) used in the present study was a mixture of *E* and *Z* geometrical isomers and was obtained from Acros Organics (purity 99%). The sample *E*:*Z* isomeric content was determined by ^{1}H NMR spectroscopy to be 91% : 9%.

For preparation of the cryogenic matrices, liquid isoeugenol was evaporated from a small glass container connected to the vacuum vessel of the cryostat via a SS-4BMRG (NUPRO) needle valve.[18] Prior to the experiment, the sample of isoeugenol was additionally purified from air and volatile impurities by pumping through the cryostat. During deposition, the valve nozzle and the sample compartment of the effusive cell were kept at the room temperature (298 K). The IE vapors were codeposited with a large excess of argon (purity N60, supplied by Air Liquide) or xenon (N48, Air Liquide) onto a CsI optical substrate of the cryostat kept at 15 K (Ar) or 30 K (Xe). Cryogenic temperatures were obtained by means of an APD Cryogenics close-cycle refrigeration system with a DE-202A expander. The temperature was measured directly at the substrate by a silicon diode sensor working with a digital controller (Scientific Instruments, model 9650-1). The conditions of the matrices deposition were chosen to avoid aggregation of IE molecules.

The IR (4000−400 cm^{-1}; 0.5 cm^{-1} resolution) spectra were recorded using a Nicolet 6700 Fourier transform infrared spectrometer, equipped with a DTGS detector and a KBr beamsplitter. The near-IR (8500−2000 cm^{-1}; 0.5 and 1 cm^{-1} resolution) spectra were recorded using the same spectrometer and detector but equipped with a CaF_2 beamsplitter.

Irradiations of the matrices were performed using the tunable UV light provided by the frequency doubled signal beam of a Quanta-Ray MOPO-SL pulsed (10 ns) optical parametric oscillator (fwhm ∼0.2 cm^{-1}, repetition rate 10 Hz, pulse energy ∼1.0 mJ) pumped with a pulsed Nd:YAG laser. For NIR irradiations, matrices were irradiated with the light provided by the idler beam of the same optical parameter oscillator.

Quantum Chemical MP2, DFT, and QCISD Calculations. All calculations were performed with Gaussian 09.[19] The B3LYP level of theory[20] with the 6-311++G(2d,2p) basis set and MP2[21] with the 6-311++G(d,p) basis set were used to obtain the structures of the relevant minima and transition states. Energies of the B3LYP optimized structures were further refined by undertaken single-point calculations using the quadratic configuration interaction with single and double excitation method (QCISD)[22] with the 6-311++G(2d,2p) basis set.

Both B3LYP/6-311++G(2d,2p) and MP2/6-311++G(d,p) harmonic vibrational frequencies and intensities were calculated at the optimized geometries. They were used for the zero-point vibrational energy corrections and thermodynamic functions calculations. The B3LYP/6-311++G(2d,2p) frequencies of the four most stable minima scaled by 0.9447, above 2000 cm^{-1}, and by 0.9817, in the 2000−500 cm^{-1} spectral region, were used to simulate their infrared spectra. The structure and the vibrational frequencies of the putative products of the UV photolysis of isoeugenol and eugenol were calculated at the B3LYP/6-311++G(2d,2p) level. The potential energy distributions (PED) of the normal modes were computed with the GAR2PED program.[23] Vibrational spectra were simulated using SYNSPEC.[24] In these simulations, the absorptions were broadened by Lorentzian profiles (fwhm = 2 cm^{-1}) and centered at the calculated (scaled) frequencies.

RESULTS AND DISCUSSION

Geometries and Energies of the IE Isomers and Isomerization Barriers. The isoeugenol molecule has two geometric isomers, *E* and *Z*, differing in the relative position of the substituents around the C═C double bond of the propenyl moiety. For each of these species, there are several conformers resulting from internal rotation about the single bonds connecting the −CH═CHCH$_3$, −OH, and −OCH$_3$ groups to the aromatic ring. Schematic representation of *E* and *Z* isoeugenol isomers is presented in Chart 2 together with the adopted atom numbering.

Chart 2. Schematic Representation of *E* and *Z* Isoeugenol Isomers, Depicting the Two Most Stable Conformers for Each Isomer (Vide Infra)

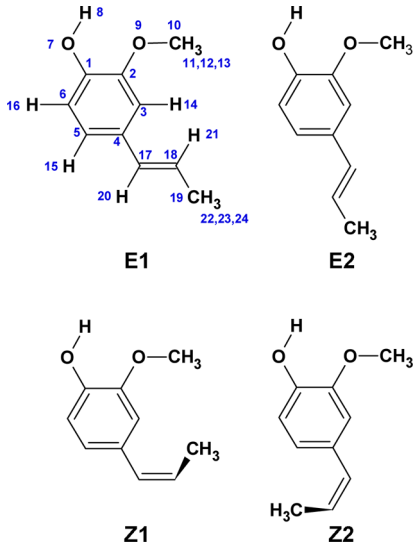

A systematic search on the B3LYP/6-311++G(2d,2p) potential energy surface (PES) of the isoeugenol molecule revealed the presence of six unique minima in case of the *E* isomer (E1−E6), and eight *Z*-type (Z1−Z8) unique minima. The four most stable *E* conformers belong to the C_s symmetry point group, being unique structures, whereas all the remaining conformers have the C_1 symmetry and possess an equivalent mirror-image form. The number of nonequivalent *E*-type

dx.doi.org/10.1021/jp306339g | J. Phys. Chem. B 2012, 116, 11148−11158

Table 1. Key Torsional Angles (deg), Zero-Point Corrected Relative Energies (ΔE_{ZPE}/kJ mol^{-1}), Barriers to Internal Rotation ($\Delta E^{\#}$/kJ mol^{-1}), Relative Gibbs Energies (ΔG_{298}/kJ mol^{-1}), and Abundances at 298 K (A_{298}, %), for the Low Energy Conformers of *E* and *Z* Isoeugenol and Transition States (TS) Connecting the Conformers of Each Isomer[a]

	B3LYP							QCISD	
	$H_8O_7C_1C_2$	$C_{10}O_9C_2C_1$	$C_3C_4C_{17}C_{18}$	$C_4C_{17}C_{18}C_{19}$	ΔG_{298}	A_{298}	ΔE_{ZPE}	ΔE_{ZPE}	
E1[b]	0.0	180.0	0.0	180.0	0.00	74.09	0.00	0.00	
E2	0.0	180.0	180.0	180.0	3.68	16.81	1.62	2.06	
Z1	0.1	-179.4	30.9	2.4	16.29	4.01	13.31	9.18	
Z2	-0.3	-179.2	148.7	-2.3	15.75	4.97	12.88	9.06	
	B3LYP							QCISD	
	$H_8O_7C_1C_2$	$C_{10}O_9C_2C_1$	$C_3C_4C_{17}C_{18}$	$C_4C_{17}C_{18}C_{19}$	ν (cm^{-1})		$\Delta E^{\#}$	ΔE_{ZPE}	$\Delta E^{\#}$
TS(E1-2)	0.0	-179.6	90.4	179.8	93i	16.56	16.56/14.94	10.12	10.12/8.05
TS(Z1-2)	0.0	-179.9	89.4	0.1	45i	19.17	5.86/6.30	10.53	1.35/1.47
	MP2								
	$H_8O_7C_1C_2$	$C_{10}O_9C_2C_1$	$C_3C_4C_{17}C_{18}$	$C_4C_{17}C_{18}C_{19}$	ΔG_{298}	A_{298}	ΔE_{ZPE}		
E1	-2.8	171.3	28.9	-179.5	0.04	45.11	0.00		
E2	-3.2	172.3	149.1	179.1	0.00	45.79	0.59		
Z1	-2.4	171.5	45.7	3.1	6.48	3.84	6.08		
Z2	-2.8	173.1	135.5	-2.7	5.75	5.15	6.07		
	MP2								
	$H_8O_7C_1C_2$	$C_{10}O_9C_2C_1$	$C_3C_4C_{17}C_{18}$	$C_4C_{17}C_{18}C_{19}$	ν (cm^{-1})		$\Delta E^{\#}$		
TS(E1-2)	-3.1	171.3	90.8	179.9	105i	10.88	10.88/10.29		
TS(Z1-2)	-3.4	171.9	90.1	0.2	48i	8.88	2.80/2.80		

[a]Both B3LYP and QCISD calculations were performed with the 6-311++G(2d,2p) basis set. QCISD calculations are single point calculations at the B3LYP optimized geometries. MP2 calculations were performed with the 6-311++G(d,p) basis set. Abundances were obtained using the calculated Gibbs free energy for the particular IE species and calculated separately for *E* and *Z* isomers taking into account the experimentally found *E*:*Z* isomeric ratio in the liquid sample used for preparation of the cryogenic matrices. For transition states, the imaginary frequency (ν/cm^{-1}) is provided. Barriers to internal rotation are given for the direct/reverse reaction. See Chart 2 for atom numbering and for structures of the minima. The extended version of this table, including data for all the calculated structures, is provided in the Supporting Information (Table S1). [b]The calculated absolute energy of E1 (global minimum) is equal to −538.88663, −537.49154, −537.30839 (hartree) at DFT, QCISD, and MP2, respectively; the DFT calculated absolute Gibbs free energy of E1 is equal to −538.72817 (hartree); the MP2 calculated absolute Gibbs free energy of E2 is equal to −537.149315 (hartree).

conformers predicted at the B3LYP level of approximation is smaller than the number of *Z*-type conformers, because in all *E* forms both the hydroxyl and propenyl groups are in the plane (or only very slightly out of the plane) of the aromatic ring, whereas in all *Z* forms the propenyl group is considerably out of the plane. On the other hand, the MP2 method predicts the propenyl group considerably out of plane for all minimum energy structures, so that at this level of theory both *Z* and *E* isomers are predicted to have eight nonequivalent-by-symmetry conformers (all of C_1 symmetry and possessing an equivalent mirror-image form).

For both *E* and *Z* isoeugenol isomers, the two most stable conformers have energies substantially lower than all the other forms. The main dihedral angles for these species are given in Table 1 (data for the remaining conformers are given in Tables S1 and S2, in the Supporting Information). The B3LYP, MP2, and QCISD (single point calculations at the B3LYP optimized geometries) relative energies of all stable IE forms and relevant transition states are also provided in Tables 1 and S1 (Supporting Information), as well as the B3LYP/6-311++G(2d,2p) and MP2/6-311++G(d,p) calculated relative Gibbs energies and abundances at 298 K. The potential energy profile for conversion between E1 and E2 and between Z1 and Z2 obtained at the DFT and MP2 levels are shown in Figure 1.

The relative populations of the IE forms in the gas phase (at 298 K) were determined using the Gibbs energy values for the particular IE species, and calculated separately for *E* and *Z* isomers taking into account the experimentally measured *E*:*Z* isomeric ratio in the liquid sample used for preparation of the cryogenic matrices (see Experimental and Theoretical Methods). The obtained abundances revealed that only the two most stable conformers of each isomer (*E*, *Z*) have practical significance, with all other forms having negligible populations (<0.05%).

According to the relative orientation of the OH and OCH_3 moieties, the different conformers can be grouped in three sets. Within each set, *E*-type conformers have lower energies than *Z*-type forms. In one set, the OH group points to the OCH_3 group, allowing for the establishment of an intramolecular OH···O(CH_3) hydrogen bond. The members of this group correspond to the four low energy conformers of IE depicted in Chart 2.

Conformer E1 corresponds to the global minimum, the relative energies ΔE_{ZPE} of E2, Z1, and Z2 being 1.62/0.59,

dx.doi.org/10.1021/jp306339g | J. Phys. Chem. B 2012, 116, 11148−11158

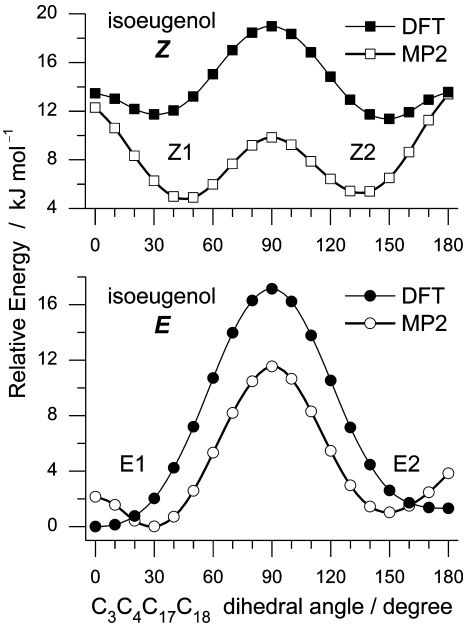

Figure 1. Relaxed potential energy profiles for internal rotation around C_4C_{17} bond calculated at the MP2/6-311++G(d,p) and B3LYP/6-311++G(2d,2p) levels. Squares (top) and circles (bottom) correspond to the *Z* and *E* isoeugenol forms, respectively. The atom numbering is presented in Chart 2. Energy of the most stable E1 form was chosen as the relative zero. Note that the linear ordinate scales in the two frames are equal.

13.31/6.08, and 12.88/6.07 kJ mol^{-1} when calculated at B3LYP/6-311++G(2d,2p) and MP2/6-311++G(d,p) levels of theory, respectively (Figure 1). The energy difference and the relative ΔG value calculated for the two most stable E1 and E2 conformers at the MP2 level are smaller than those predicted for these species at the B3LYP level. The populations of E1 and E2 in the used sample, at 298 K, were estimated at the B3LYP/6-311++G(2d,2p) level to be ca. 74.1 and 16.8%. At the MP2/6-311++G(d,p) level, the populations of E1 and E2 were predicted as 45.1 and 45.8%, respectively. The resultant MP2 abundances of E1 and E2 appeared to be almost equal, and as will be shown later, they are closer to those observed in the experiments than the predicted with the B3LYP method. A similar situation, where the MP2 method produced more precise relative energies (than B3LYP) and was in agreement with the experimental observation, was found in a recent study on tetrazole derivatives with unsaturated hydrocarbon side-chain.[25]

Both B3LYP and MP2 methods predicted almost the same stability for the Z1 and Z2 conformers and relative populations of ca. 4 and 5%, respectively. However, the energy gap separating the *E* and *Z* forms at the B3LYP level is approximately twice as large (ca. 12 kJ mol^{-1}) comparing to the MP2 (ca. 6 kJ mol^{-1}), as can be seen in Figure 1.

It is worth mentioning that the geometry of the intramolecular OH···O(CH_3) bond in all conformers belonging to this group is very much the same as that reported earlier for the eugenol molecule.[15] It is characterized by a hydrogen bond distance in the range 2.108−2.119/2.084−2.088 Å and it is, as expected for this type of interaction, far from linearity, with the O−H···O angle equal to ca. 114/116° at B3LYP/MP2, respectively. Differences in other structural parameters calculated for the various low energy IE conformers were found to be in general small, usually not exceeding 0.005 Å for bond lengths and 4° for bond angles, with the larger deviations occurring for structural parameters of the OH, OCH_3 and $CH{=}CHCH_3$ substituents, in agreement with their expected greater sensitivity to the conformational changes of the molecule.

In the other two sets of conformers of isoeugenol, the OH group points away from the OCH_3 group, whereas the methoxyl group can assume conformations where the CH_3 group is placed nearly in the plane of the aromatic ring (corresponding to a $C_{10}O_9C_2C_1$ dihedral angle of ca. 180°) or above or below that plane ($C_{10}O_9C_2C_1$ of ca. +70° or −70°). According to the B3LYP calculations, for the *E* isomer, where in all minima the OH and propenyl groups are in the plane (or only very slightly out of the plane) of the aromatic ring, the minima with positive or negative $C_{10}O_9C_2C_1$ dihedrals (ca. ± 70°) are equivalent-by-symmetry mirror images of each other, and the other two conformers are unique structures of C_s symmetry. On the other hand, as already mentioned, the MP2 calculations predict the propenyl group considerably out of plane for all minimum energy structures, both *E* and *Z*. Hence, at this level of theory for both *Z* and *E* isomers only the OH group is always placed nearly in the plane of the aromatic ring, so that the possible combinations of the different favored orientations of the OCH_3 and propenyl groups relatively to the plane of the aromatic ring lead to existence of eight different conformers (Table S1, Supporting Information). The relative B3LYP and MP2 energies of these conformers, compared to the lowest energy E1 form, are in the range 17−34 kJ mol^{-1} (Table S1, Supporting Information). Regarding the calculated QCISD relative energies, the *Z* isomer is somewhat stabilized in relation to the *E* form, comparing to the B3LYP values, and the higher energy conformers are also slightly stabilized at the higher level of theory, which accounts better for dispersion forces. These results come in line with those obtained at the MP2 level, which also account better for dispersive interactions.

A rough estimation of the strength of the intramolecular H-bond in the low energy isoeugenol conformers can be made by comparing the relative energies of the forms differing only in the orientation of the OH group relatively to the OCH_3 fragment. For all four relevant pairs of conformers (i.e., pairs of conformers E1/E3, E2/E4, Z1/Z4, and Z2/Z3) the obtained value is in the range 16.5−19 kJ mol^{-1}. This estimation of the intramolecular H-bond energy must, however, be considered only an upper bound to the real value, because the energies of the higher energy conformers shall also contain a relevant term due to the repulsive interaction between the lone electron pairs of the two oxygen atoms (which in these conformers point to each other).

Transition states joining *E*-type minima or *Z*-type minima were located on the IE ground state potential energy surface, to estimate the energy barriers separating different conformers. The results are summarized in Table 1 (only for interconversions between the most stable species) and Table S1 (Supporting Information).

The B3LYP/MP2 barriers associated with changes in the relative orientation of the propenyl moiety (driving coordinate: torsion about the C4−C17 bond) are in the range 10−16 kJ mol^{-1} in *E* species and are considerably smaller (2.5−7 kJ mol^{-1}) in the *Z* isomer. In particular, the barriers for the E2 → E1 and Z2 → Z1 conversions between the experimentally relevant species (Figure 1) are predicted at these levels of theory to be equal to 14.94/10.29 and 6.30/2.80 kJ mol^{-1},

dx.doi.org/10.1021/jp306339g | J. Phys. Chem. B 2012, 116, 11148−11158

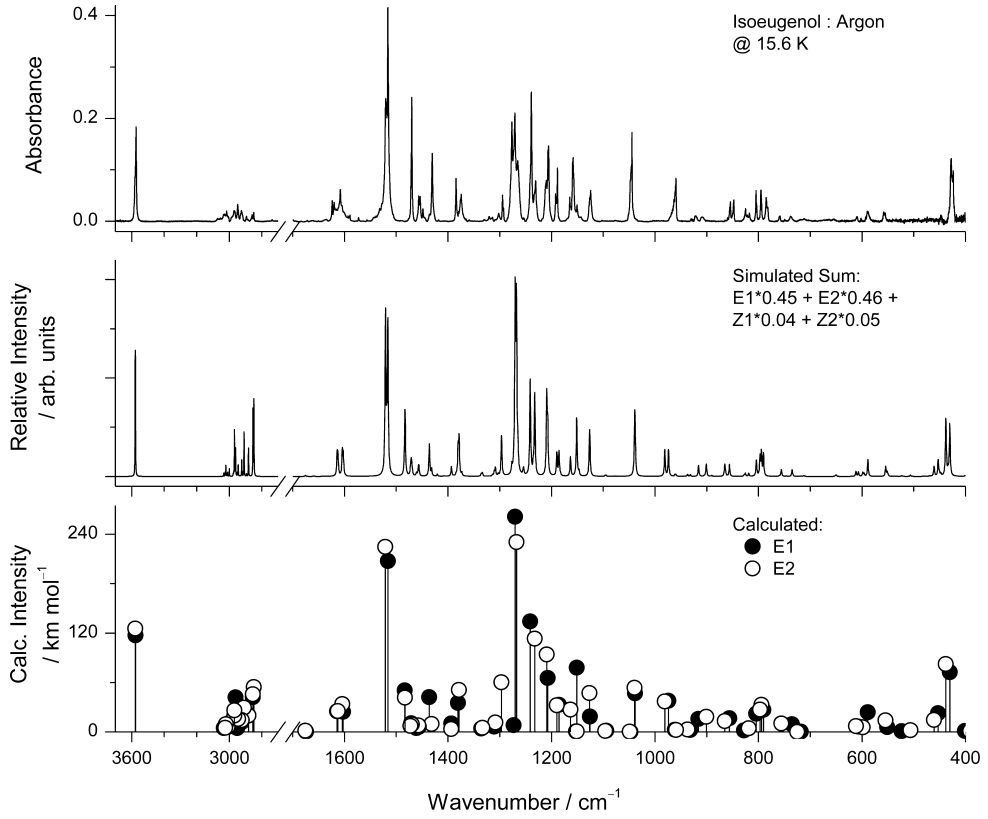

Figure 2. Infrared spectra of isoeugenol. Top: isoeugenol monomers isolated in an argon matrix at 15.6 K. Bottom: theoretical spectra of the two most stable E1 and E2 rotamers calculated at the B3LYP/6-311++G(2d,2p) level. Theoretical wavenumbers were scaled by the factors 0.9447 and 0.9817 above and below 2000 cm^{-1}, respectively. Middle: simulated sum spectrum obtained by adding the calculated (B3LYP) spectra of the four lowest energy isoeugenol rotamers whose intensities were weighted by their estimated populations (see text). In the simulations, the absorptions were broadened by Lorentzian profiles (fwhm = 2 cm^{-1}) and centered at the calculated (scaled) frequencies.

respectively (16.56/10.88 and 5.86/2.80 kJ mol^{-1} for the reverse reactions). The QCISD calculations predict somewhat lower barriers for this type of isomerizations: 8−10.5 and 1−2 kJ mol^{-1} in *E* and *Z*-isomers, respectively (Tables 1 and S1, Supporting Information).

Interconversions between conformers with different relative orientations of the hydroxyl and methoxyl group are driven by changes in the torsion about the C1−O7 or C2−O9 bonds (or both). These barriers are predicted to be similar in both *E* and *Z* isomers. In the case of the B3LYP/MP2 barriers for rotation of the OH group, they were all predicted to be in the 25−28 kJ mol^{-1} range, measured from the low energy H-bonded conformers, or about 6−9.5 kJ mol^{-1} in the inverse direction (QCISD: 23−24 and 6.2−6.6 kJ mol^{-1}, respectively). On the other hand, the barriers for rotation of the OCH_3 group are generally lower and equal to 5−8.5 kJ mol^{-1} (forward) and 3.5−5.5 kJ mol^{-1} (reverse) (QCISD: 6.5−7.5 and 4−5 kJ mol^{-1}, respectively).

The rotational barrier for conversion between *E* and *Z* forms can be expected to be very large. Generalized valence bond (GVB) calculations for ethylene gave a value of ca. 315 kJ mol^{-1} for the double bond singlet rotational barrier.[26] For *p*-(dimethylamino)-*β*-chlorostyrene, similar to the IE molecule, the activation energy for rotation around the ethylene double bond was estimated as 250 kJ mol^{-1}.[27] On the other hand, photoisomerizations about single bonds are generally easily accessible and commonly observed for matrix-isolated molecules.[28−30]

Infrared Spectrum of Freshly Deposited IE Sample in Argon Matrix. According to the performed calculations the *E*-type species with the intramolecular O−H···O hydrogen bond and with the anti arrangement of the propenyl substituent (E1 and E2) are the most stable forms of the isoeugenol molecule. The infrared spectrum of IE isolated in an argon matrix deposited at 15 K is presented in Figure 2 (upper trace) together with the sum spectrum predicted theoretically for the E1, E2, Z1, and Z2 rotamers scaled by their estimated abundance at 298 K. The populations predicted by the MP/26-311++G(d,p) method fit better to the experiment than those predicted by B3LYP/6-311++G(2d,2p) and were then used to scale intensities in the simulated spectrum. As seen from this figure, the experimental spectrum of the freshly deposited matrix is well reproduced by the theoretical spectrum consisting of all four components. However, it is also clear that, due to the expected small populations of the Z1 and Z2 forms (4−5% each), which are close to the limit of detection, and also due to the expected overlapping with the much more intense bands of the E1 and E2 species, most of the Z1 and Z2 absorptions are difficult to distinguish, and only a few bands due to the Z1 and Z2 conformers are detected as separate features in the spectra after deposition. Table S3, in the Supporting Information, presents the observed and B3LYP/6-311++G(2d,2p) calculated frequencies and IR intensities of the four most stable isoeugenol species, together with the proposed bands assignment. The interpretation of the spectra is based on the analysis of the theoretically predicted spectra and the corresponding potential energy distribution (PED) matrices. The results of the

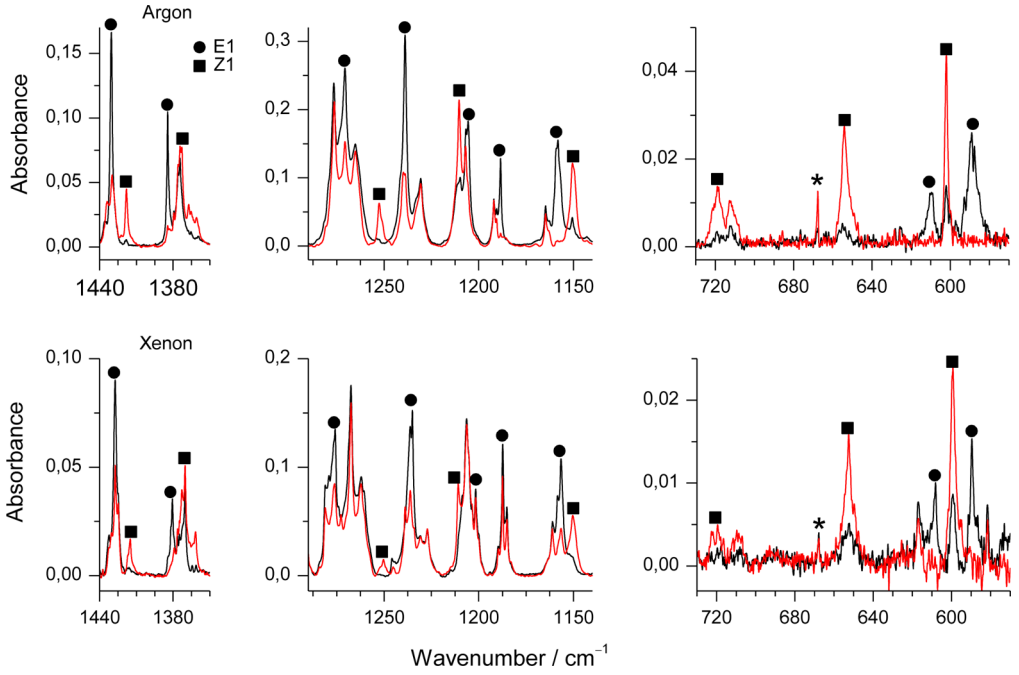

Figure 3. Selected regions of the IE spectra. Top panel: experimental spectra of freshly deposited IE/Ar matrix (black traces) and freshly deposited IE/Ar matrix taken after irradiation at 308 nm (red traces). Bottom panel: experimental spectra of freshly deposited IE/Xe matrix (black traces) and freshly deposited IE/Ar matrix taken after irradiation at 311 nm (red traces). Note formation of Z1 at the expense of E1, while bands belonging to E2 and Z2 remain unaffected. The asterisk marks the band due to traces of atmospheric CO_2.

normal coordinate analysis for E1 and the definition of the internal coordinates used in this study are given in Table S4 (Supporting Information).

Annealing of the freshly deposited IE/Ar matrices up to 30 K did not lead to any changes in the infrared spectrum that could be assigned to the conformational changes. The lack of changes upon annealing in the case of E2 → E1 transformation means that at the applied temperature the available energy is not enough to overcome a barrier above 10 kJ mol^{-1}.[31] In turn, the Z1 → Z2 or Z2 → Z1 transformations are related with a much smaller energy barrier (2.8 kJ mol^{-1}, MP2 level). However, as already mentioned, the amounts of the *Z* conformers of isoeugenol in freshly deposited matrices are very small. Together with the extensive overlapping of their bands with the intense ones due to *E* forms, this makes it impossible to conclude on the possible occurrence of these isomerizations at this stage of the experiment.

Narrow Band Tunable UV Irradiation Experiments. In a preliminary experiment, a series of UV irradiations of the IE/Ar and IE/Xe matrices was carried out using narrow band radiation, starting at 340 nm and gradually decreasing the wavelength in steps ranging from 1 to 10 nm. After each irradiation, an infrared spectrum of the matrix was taken to monitor possible transformations of the IE rotamers. The onset of photoreaction was incrementally constricted with a precision of 1 nm. Irradiations with $\lambda \geq 312$ nm did not induce any changes in the infrared spectra, whereas upon irradiation at λ = 311 nm a photoinduced reaction started to occur.

In subsequent experiments, freshly deposited samples of matrix-isolated IE were irradiated starting off the λ = 311 nm mark. In doing so, new bands started to increase slowly at the expense of the E1 absorptions. These new bands could be assigned to the Z1 species. The process speeded up upon irradiation in the λ = 310−306 nm range. The reaction was found to be similar for both argon and xenon matrices. Selected regions of the experimental spectra of the IE/Ar and IE/Xe matrices before irradiation and after a sequence of irradiations in the 311−308 nm range are shown in Figure 3. The observed spectral changes are a clear indication of conversion of the most stable E1 isomer (anti configuration around C═C bond) into the Z1 form (syn configuration). This process may be followed while looking at the kinetic profiles obtained for the E1 (1158.0 cm^{-1}) and Z1 (1418.0 cm^{-1}) bands presented in Figure 4. Note that irradiations at 308−306 nm resulted in saturation suggesting photoequilibrium.

Further irradiations at λ = 305 nm induced spectral changes that indicated occurrence in the matrix of the Z1 → E1 back-reaction. The bands associated with the Z1 isomer decreased

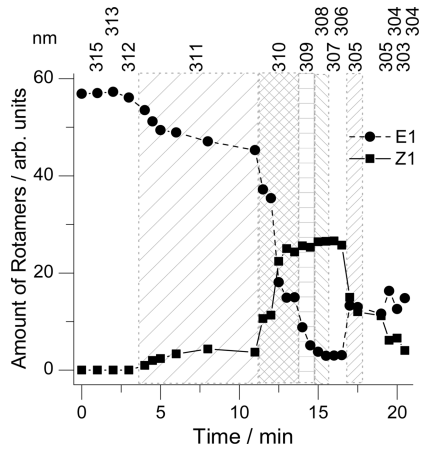

Figure 4. Kinetic profiles obtained for the E1 (1158.0 cm^{-1}) and for Z1 (1418.0 cm^{-1}) bands. In these profiles, the "amount of rotamer" is proportional to the experimental integrated band intensities divided by the calculated infrared intensity of the corresponding vibration. At the top, note the wavelengths (nm) used in the sequence of irradiations.

dx.doi.org/10.1021/jp306339g | *J. Phys. Chem. B* 2012, 116, 11148−11158

gradually in favor of the E1 absorptions. This effect is shown in Figure 5, where selected regions of the experimental spectra of

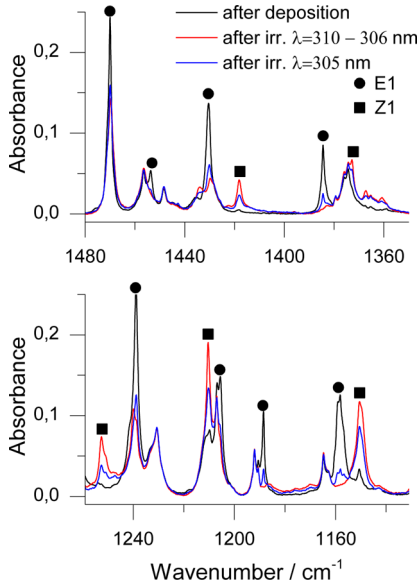

Figure 5. Selected regions of the IE/Ar experimental spectra obtained for the freshly deposited matrix (black traces) and for the freshly deposited matrix after 15 min irradiation at 310−306 nm (red traces) followed by 1 min of irradiation at λ = 305 nm (blue traces). Note the reversibility of transformation between E1 and Z1 and the fact that bands belonging to E2 and Z2 remain unaffected.

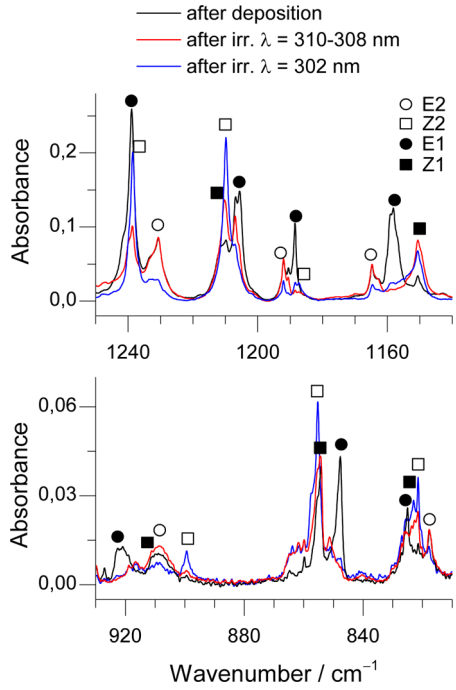

Figure 6. Selected regions of the IE/Ar experimental spectra obtained for the freshly deposited matrix (black traces) and for the freshly deposited matrix after irradiation at 310−308 nm (red traces) followed by 1 min of irradiation at λ = 302 nm (blue traces).

freshly deposited matrices (black traces) are compared with those obtained after the previously described irradiations at 310−306 nm (red traces) and followed by λ = 305 nm irradiations (blue traces). The described direct observation of the UV induced E1 → Z1 and Z1 → E1 reactions provided an undoubted proof of the photoreversibility of the E1 ↔ Z1 transformation.

The intensities of the bands belonging to both E2 and Z2 remained unaffected when the sample was irradiated with λ > 302 nm. When the sample was irradiated at 302 nm, the set of bands associated with the E2 species started to decrease in favor of the Z2 absorptions, indicating that the E2 → Z2 conversion was now taking place. Figure 6 shows selected regions of the experimental spectra obtained after λ = 310−308 nm irradiations (red traces) (E1 → Z1 transformation) and λ = 302 nm irradiation (blue traces) (E2 → Z2 transformation). For comparison, the IE/Ar spectrum after deposition (black traces) is also given. Further irradiation in the λ = 298−296 nm range allowed for a partial Z2 → E2 back-transformation to be detected, although the spectral changes induced in this case are not so pronounced as those observed for the other three isomerizations above-mentioned.

An additional study was performed that combined UV irradiation and annealing of a freshly deposited IE/Ar matrix. First, the sample was irradiated at 15 K with UV light (λ = 308 nm) to increase the population of the Z1 isomer by inducing a partial E1 → Z1 transformation. This operation resulted in selective increase of population for only one of the *Z* rotamers. Next, annealing of the matrix was performed to check on the possible conformational exchange between the Z1 and Z2 species. The annealing was carried out in steps of 2 K and, up to 26 K, the band intensities of all forms remained unchanged. At 28 K, the bands due to the photoproduced Z1 rotamer started to decrease. The bands growing at the expense of Z1 were the same as produced in the preceding experiment upon irradiation with λ = 302 nm and were assigned to Z2 species. The thermally induced Z1 → Z2 transformation was partial and after some time changes stopped, even though the sample temperature was raised up to 32 K.

Figure 7 shows the difference absorption spectra in two regions obtained by subtracting the experimental spectrum of the IE/Ar matrix after 3.5 min irradiation at 308 nm from that taken after annealing of the irradiated matrix at 32 K. These spectra are compared to the difference of the simulated spectra for the Z1 and Z2 species. Positive bands in this figure are due to the Z2 species. Figure 8 shows the kinetic profiles obtained for the Z2 (1434.0 cm^{-1}) and Z1 (1418.0 cm^{-1}) bands. On the basis of the observed spectral changes, it is clear that the population of the Z2 form increases in the matrix after annealing, indicating that the energy barrier for the Z1 → Z2 conversion, estimated to be below 2.8 kJ mol^{-1} (MP2 value; Table 1), is low enough to be surpassed at 28 K. Moreover, the fact that populations of the Z1 and Z2 forms reach saturation at approximately equal amounts (Figure 8) may indicate that these forms are isoenergetic, as predicted by the MP2 calculations. A similar annealing behavior was earlier observed for two isoenergetic conformers of 1,3-butanediol.[32]

Figure 9 presents a summary of the observed UV-induced and thermal conversions. It is worth mentioning that the attempts to induce the E2 → E1 conversion by matrix annealing were not successful. Indeed, although the energy difference between E1 and E2 is small (<1.7 kJ mol^{-1}), the energy barrier associated with the E2 → E1 conversion is, according to the calculations, relatively high (>10 kJ mol^{-1}; Table 1) and precludes the conformational cooling.[33]

Photochemistry Appearing upon the UV Narrow Band Laser Irradiation of EU/Ar and IE/Ar Matrices. It

dx.doi.org/10.1021/jp306339g | J. Phys. Chem. B 2012, 116, 11148−11158

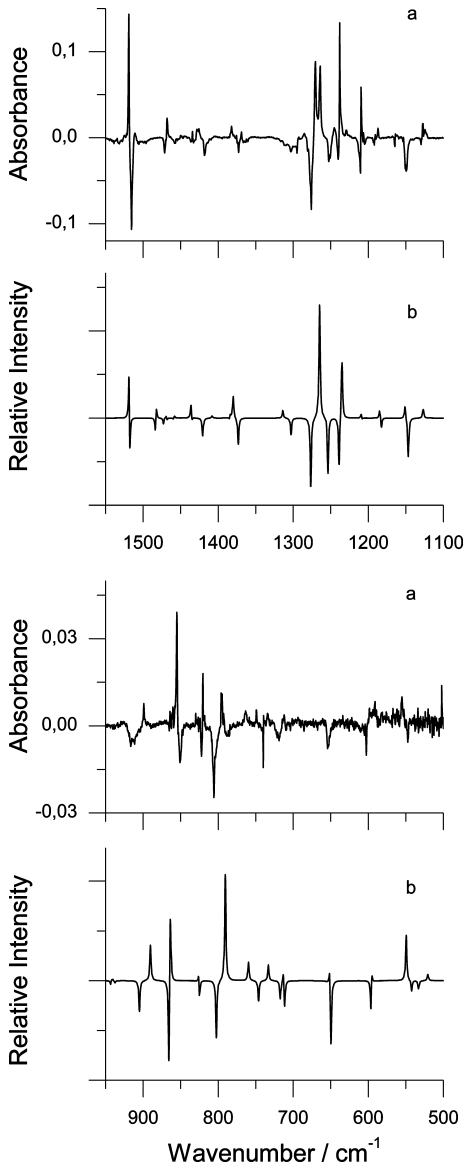

Figure 7. (a) Experimental difference spectrum obtained by subtracting the spectrum of isoeugenol in Ar matrix after 3.5 min irradiation at 308 nm at 15 K from that taken after annealing of the irradiated matrix up to 32 K. (b) Simulated difference spectrum constructed as Z2 minus Z1.

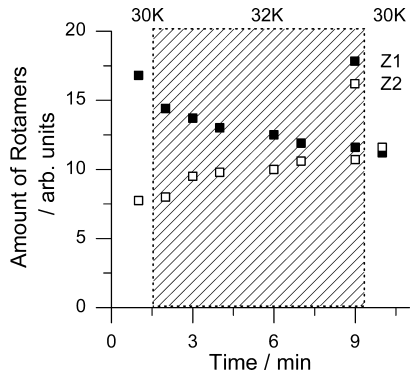

Figure 8. Kinetic profiles showing changes of populations of Z2 (1434.0 cm^{-1}) and Z1 (1418.0 cm^{-1}) rotamers in the process of annealing. In these profiles, the "amount of rotamer" is proportional to the experimental integrated band intensities divided by the calculated infrared intensity of the corresponding vibration. At the top, note the sample temperature (K).

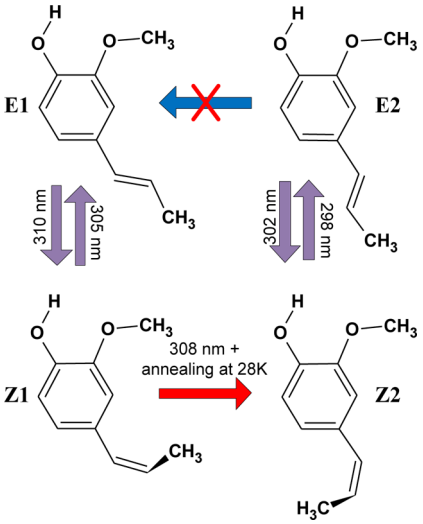

Figure 9. Light-induced and thermal interconversions occurring in the IE/Ar matrices.

is worth mentioning that similar series of irradiations with the tunable UV laser source, as described in the preceding paragraph, were also applied to eugenol (EU) isolated in argon matrices but found not to induce any conformational changes for this molecule. However, upon irradiation at λ = 308 nm the bands assigned to the EU monomer[15] started to decrease and, simultaneously, an intense new absorption due to photogenerated species appeared in the region 2150−2100 cm^{-1}, with three main maxima at 2137.0, 2133.0, and 2111.0 cm^{-1}. The components of this absorption showed somewhat different patterns of intensity changes during subsequent irradiation of the matrix with shorter wavelengths. The intensity of both the 2133.0 and 2111.0 cm^{-1} features was increasing until the 276 nm wavelength was applied but then started to decrease during the subsequent irradiations at shorter wavelengths. Simultaneously, the feature at 2137.0 cm^{-1} appeared and systematically grew up along the entire course of the photolysis experiments. At the end of the series of irradiations (λ = 250 nm), the 2133.0 and 2111.0 cm^{-1} bands vanished, whereas the intense 2137 cm^{-1} feature was the only feature observed in this region.

Figure 10 shows the evolution of the EU/Ar spectra in the discussed region during the progress of the photolysis, together with the kinetic profiles for two components (2137.5 and 2111.0 cm^{-1}) of the 2150−2100 cm^{-1} absorption and for one band of the most stable EU conformer (ca. 3574 cm^{-1}).

On the basis of the results reported for the phenol precursors[34] the photoinduced cleavage of the OH bond is the most probable transformation expected for the studied compound. Two pathways following hydrogen atom shift that are possible for the eugenol molecule are presented in Figure 11. Depending on the position of the ring where the hydrogen atom moves, the reaction leads to two different open-ring ketene molecules. Each of these ketenes (denoted as EK1 and EK2 in Figure 11) may be formed in the matrix cage in various isomeric forms. The performed B3LYP/6-311++G(2d,2p) calculations show 60 and 47 stable conformers for EK1 and EK2, respectively. Some of these structures are presented in the Supporting Information (Figure S1) together with the B3LYP/

dx.doi.org/10.1021/jp306339g | J. Phys. Chem. B 2012, 116, 11148−11158

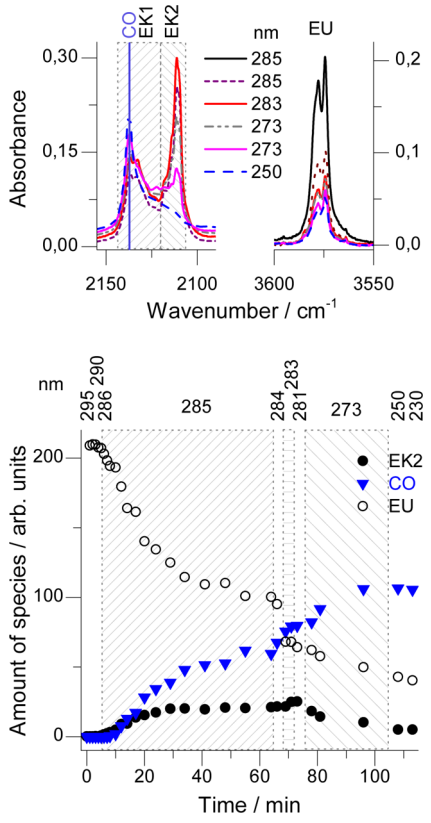

Figure 10. Evolution of the EU/Ar spectra in the 2150−2100 and 3600−3550 cm^{-1} regions during the progress of the photolysis and the kinetic profiles for the 2137.5, 2111.0, and ca. 3574 cm^{-1} bands. In these profiles, the "amount of species" is proportional to the experimental integrated band intensities divided by the calculated infrared intensity of the corresponding vibration. Note wavelengths (nm) at the top of kinetic profiles.

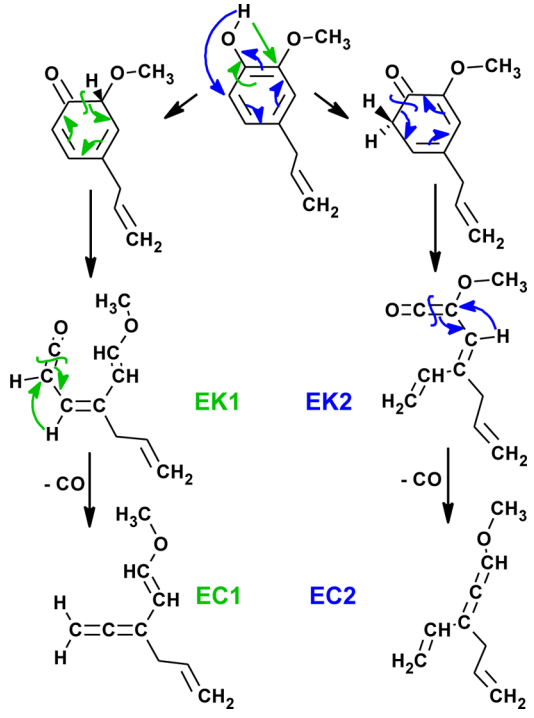

Figure 11. Photolysis pathways resulting from irradiation of the EU/Ar matrices.

6-311++G(2d,2p) positions and intensities of the most intense bands calculated for these species (Table S5, Supporting Information). According to the calculations, all the EK1 and EK2 species are characterized by a very intense band (calculated intensity in the range 700−2000 km mol^{-1}) due to the antisymmetric stretching vibration of the −C═C═O group.[34,35] This mode is predicted to appear in the 2140−2120 and 2120−2107 cm^{-1} regions (frequencies scaled by 0.981) for the different conformers of EK1 and EK2, respectively. These results fit very well to the positions of the bands found in the experimental spectra (2133.0 and 2111.0 cm^{-1}), observed in the course of the photolysis. The performed calculations also predicted that all other ketene vibrations are characterized by at least one order of magnitude lower intensities than the ν_{as}(C═C═O) mode. This fact explains why no other absorptions due to the ketene species were detected in the spectra of the irradiated matrices.

The position of the 2137 cm^{-1} band allows for its direct assignment to the vibration of the carbon monoxide molecule formed during decarbonylation of both EK1 and EK2 ketene molecules (Figure 10). A consequence of these photofragmentations is the formation of two types of compounds with cumulated and conjugated C═C bonds (denoted as EC1 and EC2). These species were not detected in the present spectra. However, according to the calculations performed for different conformers of EC1 and EC2 these species are characterized by giving rise to infrared bands of very low intensity.

Similar photochemical reactions as described above for eugenol were detected for isoeugenol isolated in argon matrices (Figure 12, Figure S2 and Table S5 in Supporting Information). These reactions were observed in addition to the spectral changes characteristic of the above-described photoisomerizations, which were the main processes appearing upon UV irradiation of matrix-isolated isoeugenol. Although the threshold energy for the hydrogen atom shift in IE is lower compared with EU (308 nm vs 285 nm) the main features of the absorptions appearing in the spectra of the two photolyzed compounds were similar.

CONCLUSIONS

A matrix isolation study of the infrared spectra and structure of monomeric isoeugenol, one of the most important plant phenols, has been carried out. The detailed analysis of the results, supported by theoretical calculations undertaken at different levels of theory, allowed for the interpretation of the spectra and revealed the presence in the as-deposited matrices of the four most stable IE forms (E1, E2, Z1, and Z2). These species are stabilized by an intramolecular hydrogen bond between the OH group and the oxygen atom of the methoxy group. Two of these structures are characterized by the anti (*E*) configuration around C═C bond, whereas the other two forms have syn (*Z*) arrangement about this bond.

The narrow band tunable laser technique has been used to induce photorotamerization processes between the IE species. Depending on the wavelength of the laser used, different transformations were promoted, as manifested by the growth or decrease of the bands associated with particular isomers/conformers. Upon irradiation in the 311−308 nm range, the anti−syn transformation E1 → Z1 was detected, whereas irradiation at 305 nm induced the corresponding syn−anti Z1 → E1 back-reaction. Shorter wavelength irradiations (302 and 298 nm) were found to induce similar transformations between

dx.doi.org/10.1021/jp306339g | J. Phys. Chem. B 2012, 116, 11148−11158

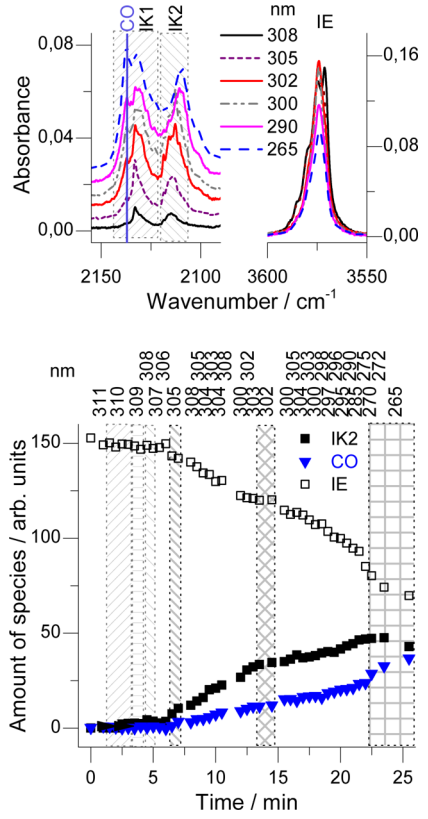

Figure 12. Evolution of the IE/Ar spectra in the 2160−2080 and 3600−3550 cm^{-1} regions during the progress of the photolysis and the kinetic profiles for the 2131.5, 2108.5, and ca. 3571 cm^{-1} bands. In these profiles, the "amount of species" is proportional to the experimental integrated band intensities divided by the calculated infrared intensity of the corresponding vibration. Note wavelengths (nm) at the top of kinetic profiles.

the second pair of anti and syn isomers (E2, Z2). In addition to the isomerizations taking place upon UV irradiation, the thermally induced Z1 → Z2 transformation was observed, in agreement with the low value of the predicted energy barrier for this process (below 2.8 kJ mol^{-1}, according to the MP2 calculations). This partial transformation started when the Z1 form was in excess (as a result of UV-irradiation) and finished when the Z1 and Z2 forms reached equal amounts, thus suggesting that these two forms are isoenergetic.

The narrow band UV irradiation technique was also applied to study the photochemistry of eugenol and isoeugenol monomers isolated in argon matrices. On the basis of the obtained results for both molecules, H-atom shift from the OH group was found to be the primary photochemical process, leading to two different long chain ketene derivatives, depending on the position of the ring to where the hydrogen atom moves. These species are characterized by very intense ν_{as}(C═C═O) bands appearing in the 2150−2100 cm^{-1} region. In addition, the carbon monoxide absorption (2137 cm^{-1}) also appears in the course of the irradiation experiments, indicating that decarbonylation of the ketenes takes also place in the photolyzed IE/Ar and EU/Ar matrices.

■ ASSOCIATED CONTENT

Ⓢ Supporting Information

Figure S1, B3LYP/6-311++G(2d,2p) optimized structures for eugenol and isoeugenol photolysis products. Figure S2, photolysis pathways resulting from irradiation of the IE/Ar matrices. Table S1, key torsional angles, zero-point energy corrected relative energies, barriers to internal rotation, relative Gibbs energies, and abundances at 298 K for the conformers of *E* and *Z* isoeugenol and transition states. Table S2, Cartesian coordinates of IE rotamers calculated at B3LYP/6-311++G(2d,2p) and MP2/6-311++G(d,p) levels of theory. Table S3, experimental and calculated frequencies and intensities of isoeugenol rotamers in argon matrices. Table S4, normal coordinate analysis results and definition of internal coordinates. Table S5, B3LYP/6-311++G(2d,2p) frequencies and intensities of the most intense bands of the photolysis products of eugenol and isoeugenol. This material is available free of charge via the Internet at http://pubs.acs.org.

■ AUTHOR INFORMATION

Corresponding Author

*M.W.: e-mail, maria.wierzejewska@chem.uni.wroc.pl; phone, +4871 3757332; fax, +4871 3282348. I.R.: e-mail, reva@qui.uc.pt; phone, +351 239854489; fax, +351 239827703.

Notes

The authors declare no competing financial interest.

■ ACKNOWLEDGMENTS

The research leading to these results has received funding from the European Community's Seventh Framework Programme under grant agreement No. 228334, and the Portuguese "Fundação para a Ciência e a Tecnologia" (FCT) Projects PTDC/QUI-QUI/111879/2009 and PTDC/QUI-QUI/118078/2010, FCOMP-01-0124-FEDER-021082, cofunded by QREN-COMPETE-UE. A grant of computer time from the Wrocław Center for Networking and Supercomputing is gratefully acknowledged.

■ REFERENCES

(1) Burt, S. *Int. J. Food Microbiol.* **2004**, *94*, 223−253.
(2) Ismail, A.; Marjan, Z. M.; Foong, C. W. *Food Chem.* **2004**, *87*, 581−586.
(3) Atsumi, T.; Fujisawa, S.; Tonosaki, K. *Toxicol. In Vitro* **2005**, *19*, 1025−1033.
(4) Veldhuizen, E. J. A.; Tjeerdsma-Van Bokhoven, J. L. M.; Zweijtzer, C.; Burt, S. A.; Haagsman, H. P. *J. Agric. Food Chem.* **2006**, *54*, 1874−1879.
(5) Burt, S. A.; Fledderman, M. J.; Haagsman, H. P.; van Knapen, F.; Veldhuizen, E. J. A. *Int. J. Food Microbiol.* **2007**, *119*, 346−350.
(6) Greenberg, M.; Dodds, M.; Tian, M. *J. Agric. Food Chem.* **2008**, *56*, 11151−11156.
(7) Hoffmann, T.; Kurtzer, R.; Skowranek, K.; Kießling, P.; Fridman, E. *Met. Eng.* **2011**, *13*, 527−531.
(8) Dambolena, J. S.; Zygadlo, J. A.; Rubinstein, H. R. *Int. J. Food Microbiol.* **2011**, *145*, 140−146.
(9) Southwell, I. A.; Russell, M. F.; Davies, N. W. *Flav. Fragr. J.* **2011**, *26*, 336−340.
(10) Ayala-Zavala, J. F.; Gonzalez-Aguilar, G. A.; Del-Toro-Sanchez, L. *J. Food Sci.* **2009**, *74*, 84−91.
(11) Cortes Cabrera, A.; Prieto, J. M. *Food Chem.* **2010**, *118*, 141−146.
(12) Tylli, H.; Konschi, H. *J. Mol. Struct.* **1988**, *176*, 245−251.
(13) Wu, R.; Brutschy, B. *Chem. Phys. Lett.* **2004**, *390*, 272−278.
(14) Dorofeeva, O. V.; Shishkov, I. F.; Karasev, N. M.; Vilkov, L. V.; Oberhammer, H. *J. Mol. Struct.* **2009**, *933*, 132−141.
(15) Olbert-Majkut, A.; Wierzejewska, M. *J. Phys. Chem. A* **2008**, *112*, 5691−5699.
(16) Longarte, A.; Unamuno, I.; Fernández, J. A.; Castaño, F.; Redondo, C. *J. Chem. Phys.* **2004**, *121*, 209−219.

(17) Castro, H. T.; Martínez, J. R.; Stashenko, E. *Molecules* **2010**, *15*, 5012−5030.
(18) Reva, I. D.; Lopes Jesus, A. J.; Rosado, M. T. S.; Fausto, R.; Eusébio, M. E.; Redinha, J. S. *Phys. Chem. Chem. Phys.* **2006**, *8*, 5339−5349.
(19) Frisch, M. J.; Trucks, G. W.; Schlegel, H. B.; Scuseria, G. E.; Robb, M. A.; Cheeseman, J. R.; Scalmani, G.; Barone, V.; Mennucci, B.; Petersson, G. A.; Nakatsuji, H.; Caricato, M.; Li, X.; Hratchian, H. P.; Izmaylov, A. F.; Bloino, J.; Zheng, G.; Sonnenberg, J. L.; Hada, M.; Ehara, M.; Toyota, K.; Fukuda, R.; Hasegawa, J.; Ishida, M.; Nakajima, T.; Honda, Y.; Kitao, O.; Nakai, H.; Vreven, T.; Montgomery, J. A., Jr.; Peralta, J. E.; Ogliaro, F.; Bearpark, M.; Heyd, J. J.; Brothers, E.; Kudin, K. N.; Staroverov, V. N.; Kobayashi, R.; Normand, J.; Raghavachari, K.; Rendell, A.; Burant, J. C.; Iyengar, S. S.; Tomasi, J.; Cossi, M.; Rega, N.; Millam, N. J.; Klene, M.; Knox, J. E.; Cross, J. B.; Bakken, V.; Adamo, C.; Jaramillo, J.; Gomperts, R.; Stratmann, R. E.; Yazyev, O.; Austin, A. J.; Cammi, R.; Pomelli, C.; Ochterski, J. W.; Martin, R. L.; Morokuma, K.; Zakrzewski, V. G.; Voth, G. A.; Salvador, P.; Dannenberg, J. J.; Dapprich, S.; Daniels, A. D.; Farkas, Ö.; Foresman, J. B.; Ortiz, J. V.; Cioslowski, J.; Fox, D. J. *Gaussian 09*, Revision C.01; Gaussian, Inc.: Wallingford, CT, 2010.
(20) (a) Becke, A. D. *Phys. Rev. A* **1988**, *38*, 3098−3100. (b) Becke, A. D. *J. Chem. Phys.* **1993**, *98*, 5648−5652. (c) Lee, C. T.; Yang, W. T.; Parr, R. G. *Phys. Rev. B: Condens. Matter* **1988**, *37*, 785−789. (d) Vosko, S. H.; Wilk, L.; Nusair, M. *Can. J. Phys.* **1980**, *58*, 1200−1211.
(21) (a) Møller, C.; Plesset, M. S. *Phys. Rev.* **1934**, *46*, 0618−0622. (b) Head-Gordon, M.; Pople, J. A.; Frisch, M. J. *Chem. Phys. Lett.* **1988**, *153*, 503−506. (c) Saebø, S.; Almlöf, J. *Chem. Phys. Lett.* **1989**, *154*, 83−89. (d) Frisch, M. J.; Head-Gordon, M.; Pople, J. A. *Chem. Phys. Lett.* **1990**, *166*, 275−280. (e) Frisch, M. J.; Head-Gordon, M.; Pople, J. A. *Chem. Phys. Lett.* **1990**, *166*, 281−289. (f) Head-Gordon, M.; Head-Gordon, T. *Chem. Phys. Lett.* **1994**, *220*, 122−128.
(22) (a) Pople, J. A.; Seeger, R.; Krishnan, R. *Int. J. Quantum Chem.* **1977**, *Suppl. Y-11*, 149−163. (b) Raghavachari, K.; Schlegel, H. B.; Pople, J. A. *J. Chem. Phys.* **1980**, *72*, 4654−4655. (c) Raghavachari, K.; Pople, J. A. *Int. J. Quantum Chem.* **1981**, *20*, 1067−1071.
(23) Martin, J. M. L.; Van Alsenoy, C. *GAR2PED*; University of Antwerp: Antwerpen, Belgium, 1995.
(24) Irikura, K. K. *Computational Thermochemistry: Prediction and Estimation of Molecular Thermodynamics*; National Institute of Standards and Technology: Gaithesburg, MD 20899, USA, 1995.
(25) Frija, L. M. T.; Reva, I.; Ismael, A.; Coelho, D. V.; Fausto, R.; Cristiano, M. L. S. *Org. Biomol. Chem.* **2011**, *9*, 6040−6054.
(26) Wang, Y.; Poirier, R. A. *J. Comput. Chem.* **1996**, *17*, 313−325.
(27) Chattopadhyay, N.; Reva, I.; Lapinski, L.; Fausto, R.; Arnaut, L. G.; Formosinho, S. J. *J. Phys. Chem. A* **2002**, *106*, 3722−3726.
(28) Lapinski, L.; Rostkowska, H.; Reva, I.; Fausto, R.; Nowak, M. J. *J. Phys. Chem. A* **2010**, *114*, 5588−5595.
(29) Kuş, N.; Sharma, A.; Reva, I.; Lapinski, L.; Fausto, R. *J. Phys. Chem. A* **2010**, *114*, 7716−7724.
(30) Kuş, N.; Reva, I.; Fausto, R. *J. Phys. Chem. A* **2010**, *114*, 12427−12436.
(31) Reva, I.; Simão, A.; Fausto, R. *Chem. Phys. Lett.* **2005**, *406*, 126−136.
(32) Rosado, M.T. S.; Lopes Jesus, A. J.; Reva, I. D.; Fausto, R.; Redinha, J. S. *J. Phys. Chem. A* **2009**, *113*, 7499−7507.
(33) Lopes Jesus, A. J.; Rosado, M. T. S.; Reva, I.; Fausto, R.; Eusébio, M. E.; Redinha, J. S. *J. Phys. Chem. A* **2006**, *110*, 4169−4179.
(34) Giuliano, B. M.; Reva, I.; Lapinski, L.; Fausto, R. *J. Chem. Phys.* **2012**, *136*, 024505.
(35) Breda, S.; Reva, I.; Fausto, R. *J. Phys. Chem. A* **2012**, *116*, 2131−2140.